We are IntechOpen,
the world's leading publisher of
Open Access books
Built by scientists, for scientists

6,900
Open access books available

186,000
International authors and editors

200M
Downloads

Our authors are among the

154
Countries delivered to

TOP 1%
most cited scientists

12.2%
Contributors from top 500 universities

CLARIVATE ANALYTICS
BOOK CITATION INDEX
INDEXED

WEB OF SCIENCE™

Selection of our books indexed in the Book Citation Index
in Web of Science™ Core Collection (BKCI)

Interested in publishing with us?
Contact book.department@intechopen.com

Photon-Upconverting Materials: Advances and Prospects for Various Emerging Applications

Manoj Kumar Mahata, Hans Christian Hofsäss and
Ulrich Vetter

Additional information is available at the end of the chapter

Abstract

Rare-earth-doped upconversion materials, featuring exceptional photophysical properties including long lifetime, sharp emission lines, large anti-Stokes shift, low autofluorescence of the background, and low toxicity, are promising for many applications. These materials have been investigated extensively since the 1960s and employed in many optical devices. However, due to rapid development of synthesis strategies for nanomaterials, upconversion materials have been rehighlighted on the basis of nanotechnology. Herein, we discuss the recent advances in upconversion materials. We start by considering energy transfer processes involved in the basic study of upconversion emission phenomena, as well as synthesis strategies of these materials. Progress in different energy transfer processes, which play an important role in determining luminescence efficiency, is then discussed. Newer applications of these materials have been vastly reviewed.

Keywords: upconversion, luminescence, rare earth, 4f-4f transitions, nanomaterials, energy transfer, optical applications, nanophosphor

1. Introduction

Photon upconversion (UC) is a nonlinear optical process which yields high-energy photons through sequential absorption of two or more low-energy photons. The concept of UC was conceived by physicist N. Bloembergen [1] in 1959 to develop an infrared (IR) photon detector for counting infrared photons through the interaction of infrared (IR) photons with rare earth (RE) or transition-metal ions incorporated in crystalline materials. Though, due to the lack of

coherent pumping sources, the prospect of achieving upconversion was not possible. With the advances in lasers and optical technology, the landmark experiment to observe IR to visible upconversion was reported first time by F. Auzel [2] in 1966 and explained energy transfer in Er^{3+}-Yb^{3+} and Tm^{3+}-Yb^{3+} systems. Since then, research on photon upconversion has inspired the design of near-infrared (NIR) to visible upconverter suitable for a wide range of applications. Later, technological advances in laser and optical tools compelled the application of upconversion lasers for converting low-energy laser radiation to high-energy laser radiation [3]. However, in early days, applications of UC materials in biomedical fields were not clear [4]. One of the major challenges was to control the size and shape of the materials that are suitable in biological environments.

Rare earth elements, including scandium and yttrium, are important in functional materials due to their similar electronic configurations ($[Xe]4f^{n-1}5d^{0-1}6s^2$). Because of this, they have similar physical and chemical properties in their trivalent ionic state. The energy levels of RE^{3+} from the 4f electronic configuration are abundant and thus allow for many intraconfigurational transitions (**Figure 1**). The intra-4f transitions are forbidden for free RE ions but these rules are partially broken when the REs are embedded in an inorganic lattice. Owing to many energy levels with intraconfigurational transitions, RE-ions act as promising luminescent centers. Moreover, the intrinsic character of RE ions due to shielding of partially filled 4f electrons by completely filled $5s^25p^6$ subshells makes them less sensitive to the environment of the host lattice. Apart from this, long life, sharp emission lines, large anti-Stokes shift, and photostability are the results of their unique 4f energy levels.
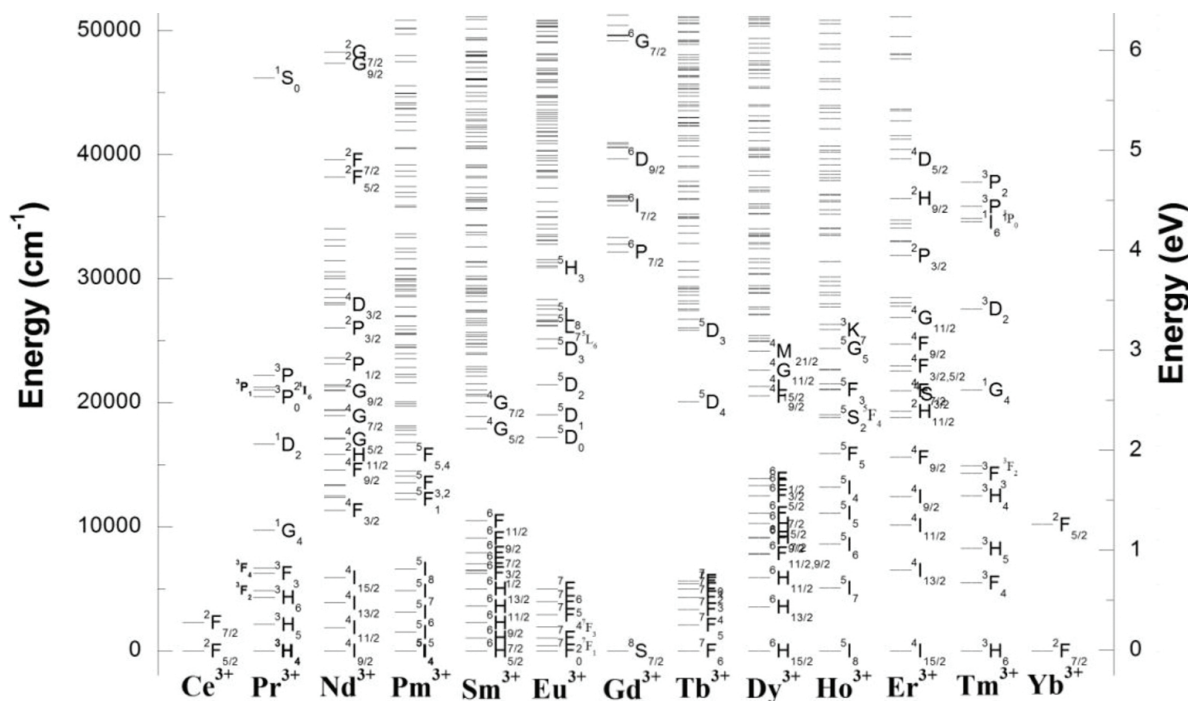

Figure 1. The 4f energy level diagrams, computed using the mean free ion parameters described in Ref. [5]. The levels were cut at 52,000 cm^{-1}.

In recent decades, UC materials have attracted much attention because of their special spectroscopic properties [6]. RE-doped luminescent materials have been employed in display devices and solid state lasers for long time. With the development of new synthesis strategies, RE-doped UC materials can be prepared at nanoscale for better prospects [3]. The emission bands of UC nanomaterials are less affected by the particle size unlike quantum dots, whose luminescence is dependent on particle size. Moreover, owing to their high resistance to photobleaching, photoblinking, specific NIR excitation, excellent penetration depth in biosystems without any autofluorescence from the background, UC particles have a wide range of applications in bioimaging and theranostics [7]. In spite of these features, several aspects of the UC nanomaterials are of great concern, such as enhancing UC efficiency, color outputs, and manipulation of energy transfer pathways to achieve desired UC emissions for specific applications.

Here, we review the recent advances in photon-upconverting materials. In this chapter, we discuss the composition of ideal UC materials, synthesis of UC particles, physics of UC followed by their applications and future prospects.

2. Composition of upconversion materials

Upconverting particles are generally composed of a host material doped with optically active sensitizer and activator ions [8]. Controlling the energy transfer processes among these three constituents is of great importance in selecting suitable dopant-host pairs. The host matrices differ in their coordination numbers, distances between dopants, and efficiencies of energy transfer. Thus proper selection of the host matrix is of significant importance. Host matrices must possess low-phonon energies to avoid degradation of efficiency through nonradiative relaxations and should be chemically and thermally stable. Moreover, host materials should have high tolerance for sensitizer and activator ions and high transparency for free migration of NIR photons in the lattice. Fluoride materials meet these criteria and are popular choices as host matrices for UC materials [8]. Among the reported host matrices, the $NaREF_4$ series has been proven to be highly effective due to their lower phonon energy and excellent chemical stability. In this family, the hexagonal-$NaREF_4$ series is more efficient than the cubic-$NaREF_4$ series due to its unique crystal structure. Oxide materials such as ZrO_2, Y_2O_3, vanadates (e.g., YVO_4, $GdVO_4$), phosphates (e.g., $LuPO_4$, YPO_4) are also examples of some common host materials because of their high chemical stability, even though they have larger phonon energies than the fluoride materials [6, 8].

The role of sensitizers is to sensitize the activators in the UC materials. An ideal sensitizer should have large absorption cross-section at the desired excitation wavelength and resonant energy levels to those of the activators, with suitable excited energy state located in the NIR region. Among all the RE ions, Yb^{3+} is the best choice as a sensitizer. The absorption cross-section of Yb^{3+} is 9.11×10^{-21} cm^{-2} at 980 nm, which is relatively large among RE ions [9]. Moreover, the energy level diagram of Yb^{3+} has only one excited state ($^2F_{5/2}$) that matches very well with the f-f transitions of many RE activators, e.g., Er^{3+}, Ho^{3+}, Tm^{3+}, etc. and therefore Yb^{3+}

is an excellent sensitizer to transfer energy to other RE ions. For example, the $^2F_{5/2}$ state of Yb^{3+} overlaps the $^4I_{11/2}$ state of Er^{3+}, allowing Yb to Er energy transfer (**Figure 1**).

UC emission increases with doping concentration of activator ions until a critical concentration. Beyond that concentration, quenching among activator ions occurs and decreases the upconversion emission [10]. To get rid of this problem, concentrations of activators are kept low while one or more types of RE ions with high concentration are incorporated as sensitizers. The activators should possess a large number of metastable energy levels. Once ground state electrons are excited to the metastable state, activators are likely to accept energy from nearby sensitizers to be excited at higher excited states. The energy levels of the activators should not be close enough to promote nonradiative relaxations. According to the energy level structures, Er, Tm, and Ho ions in their trivalent state are ideal to minimize nonradiative relaxations, whose transition rate decreases exponentially with increasing energy gap.

3. Synthesis of upconversion materials

In order to achieve high UC efficiency, synthesis of UC materials is very crucial. Recently, various methods have been developed for synthesizing RE-doped UC materials, including thermal decomposition, coprecipitation, hydrothermal, sol-gel, combustion, microwave, microemulsion, and so on [11–20]. The methods are to address specific requirements such as surface modification and monodispersity. The synthesis routes are not mutually exclusive, and often more than one method is combined to produce the suitable UC particles. Some important synthesis processes for preparing UC particles are discussed below.

3.1. Thermal decomposition

Thermal decomposition gives size-controlled well-shaped particles within short reaction time [11]. It usually involves surfactant-assisted decomposition of precursors in high-boiling organic solvents. Then the generated ions are combined into new nuclei at relatively high temperature. The trifluoroacetate and oleate compounds are commonly used organic precursors and polar capping groups such as oleic acid, oleylamine and octadecene are usually used as surfactants. It is believed that the solvents can control the growth of the particles via capping the surface of UC particles. A systematic investigation on the growth mechanism of UC nanocrystals was performed by Mai et al. [12] and inferred the passage of precursors in surfactant solutions through a slow nucleation pathway. They also showed that various sizes and shapes of Er^{3+}/Yb^{3+} doped $NaYF_4$ particles can be obtained by varying reaction time, reaction temperature, and concentration of reagents. Though this method has several important advantages, e.g., strong UC emission, high quality of products and pure phase crystals, it suffers from some disadvantages including operation difficulty, production of toxic materials, and presynthesis of $RE(CF_3COO)_3$ precursors.

3.2. Coprecipitation

The coprecipitation method is developed to overcome the limitations of the thermal decomposition method and considered as a significant method for synthesis of UC particles. It involves the precipitation of two substances simultaneously. In the coprecipitation route, UC nanocrystals are formed with organic surfactants and prevent agglomeration though their adsorption to the surface of the particles [6]. The benefits of the coprecipitation method include absence of toxic by-products, inexpensive equipment, and simple procedure. Er^{3+}/Yb^{3+}, Ho^{3+}/Yb^{3+}, and Tm^{3+}/Yb^{3+} doped LaF_3 nanoparticles [13] with particle size of 5 nm were prepared by Yi et al. In addition to that, RE-doped $LuPO_4$, $YbPO_4$, $NaYF_4$, $NaGdF_4$, and $Y_3Al_{15}O_{12}$ (YAG) nanoparticles were also produced using this method. Recently, our group has synthesized the Er^{3+}/Yb^{3+} doped $BaTiO_3$ [14] and YVO_4 [15] nanocrystals using the coprecipitation method. Despite the general advantages, this method suffers from the long-time operation of the experimental procedure, which sometimes takes more than 8 h. Moreover, to produce UC particles in industrial scales, this method is not suitable.

3.3. Hydrothermal

Thermal decomposition can only use organic solvents while hydrothermal synthesis which is mainly a solution-based method, can occur in a water-based system with low reaction temperature (around 200°C) in a relatively environment friendly condition [11]. Hydrothermal methods involve heating of the solvent at high pressure above its critical point. This process is convenient to produce controllable size and shape of the inorganic nanoparticles with diverse nanodimensional architectures. For example, yttrium orthovanadate (YVO_4) crystals have been prepared hydrothermally in both acidic and basic media with well-defined microcrystals with clear facets and dispersed nanograins and nanoflakes within 5–50 nm dimension [16]. Prism, disk, rod, and tube like $NaYF_4$ crystals were prepared by hydrothermal method [17]. An advantage of this route is that experimental parameters such as reaction temperature, reaction time, solvent type, and surfactant type can be varied to control the size and shape of the synthesized particles.

3.4. Sol-gel

The sol-gel method is generally used for the preparation of thin films, oxides, and fluoride nanocrystals [11]. The method is a typical wet-chemical process, starts with liquid solution of molecular precursors and it forms a new sol phase through hydrolysis and polycondensation reactions. With the addition of base, the sol is agglomerated into gel through a large macromolecular network, followed by annealing at high temperature for a few hours. Annealing increases crystallinity and removes the solvents from the gel. Patra et al. [18] prepared Er^{3+} doped TiO_2 and $BaTiO_3$ using basic acetate and titanium tetraisopropoxide. Patra et al. [19] developed the sol-gel method into sol emulsion-gel method to synthesize ZrO_2:Er^{3+} nanoparticles. A thin film of YVO_4:Eu^{3+} was fabricated by Cheng et al. [20] through the combination of pechini-type sol-gel method and inkjet printing. The key step in a sol-gel process is the annealing procedure. The quality of the synthesized materials is significantly dependent on the annealing temperature and time. The materials produced via sol-gel method yield high

UC intensity and the method can be applied for production on a large scale. However, there are some shortcomings in this process. For instance, the derived particles are of irregular shapes, sizes, and are not water-soluble.

3.5. Combustion

Compared to thermal decomposition, hydrothermal, and sol-gel methods, combustion synthesis is a high-throughput method of producing UC particles within a very short period of time [7]. A balanced mixture of reducing agent (fuel) and oxidizers (metal nitrates) is usually selected for the reaction to release maximum energy during the reaction time. In this process, a series of controlled explosions take place in the reaction materials in a self-sufficient condition without requiring any extra heat for the total reaction. Generally, the oxide and oxysulfide materials are prepared through this technique. Some reports on producing RE-doped Y_2O_3, La_2O_2S, Gd_2O_3, and $Gd_2Ga_5O_{12}$ can be found in the literature [6, 11]. One should keep in mind that the fuel and nitrates are chosen so that they do not produce toxic gases and the reaction should be relatively mild. However, combustion synthesis is a readily scalable, time and energy-saving, low cost, and efficient process that can be extended for commercial purpose.

4. Physics of upconversion

4.1. Upconversion mechanisms

Several mechanisms have been identified to be involved in UC process either alone or in combination [3, 4, 6, 10]. Though much work has been performed to know the energy transfer processes during UC event, only the basic possibilities, namely excited state absorption (ESA), energy transfer UC (ETU), photon avalanche (PA), cooperative UC (CUC), and energy migration-mediated UC (EMU) are given here. **Figure 2** depicts the basic UC processes.
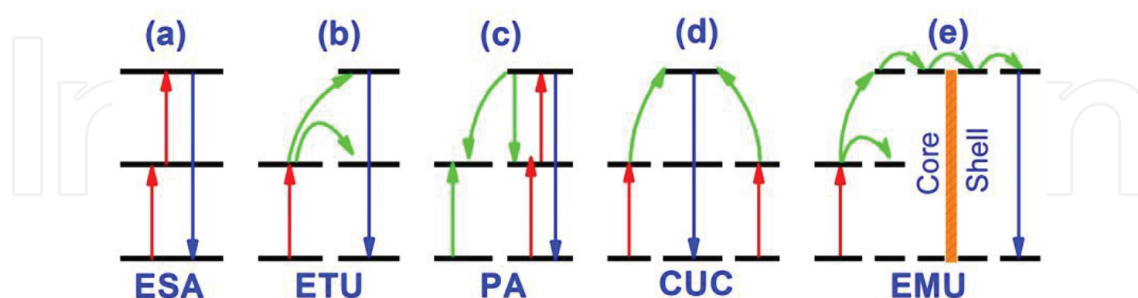

Figure 2. Simplified energy level diagrams describing upconversion processes: (a) ESA, (b) ETU, (c) PA, (d) CUC, and (e) EMU (red: excitation; blue: UC emission; green: energy transfer).

An ESA (**Figure 2a**) process refers to multistep excitation by sequential absorption of one or more low-energy photons from the ground state to intermediate state, and finally populates the intermediate state, from which upconversion emission occurs. The absorption cross-section of the excited ion should have the capability of absorbing the second pump photon. The ESA

process generally occurs at low doping concentration (<1%) of the activator ions, as high doping concentration is likely to degrade the UC emission via nonradiative relaxation processes. Although the ESA process occurs in single RE ions, its efficiency is strongly suppressed due to weak absorption induced by parity-forbidden 4f-4f transitions within RE ions.

The ETU process (**Figure 2b**) is more efficient than ESA and it involves two types of luminescent centers—sensitizer and activator ions. Once the sensitizer is excited, it transfers energy to the nearest activator ion and UC emission is obtained from the activator when it drops back to the ground state or lower excited state. For sufficient energy transfer, the activator and sensitizer should possess resonant energy levels with closeness in spatial distance between them. Because of resonant energy absorption, the excitation lifetime is longer and probability of UC is higher which makes this process an efficient one.

The PA process (**Figure 2c**) is more complex than the ESA and ETU and only occurs after a critical level of pump density. The PA process was first proposed in 1979 using Pr^{3+} ion-based infrared quantum counter. If the pump density is sufficiently high, the intermediate reservoir level of many ions becomes populated initially by a nonresonant ground state absorption process, followed by resonant ESA or ETU from another excited ion to populate the UC emitting level. After this stage efficient cross relaxation takes place between excited and ground-state ions. As a result, population of the reservoir level and the UC emitting level increases and causes an "avalanche" effect of generating more excited ions through feedback looping, making this process the most efficient.

The CUC process (**Figure 2d**) is similar to ETU process and includes two types of luminescent centers—sensitizer and activator. In this process the UC emitting level of the activator is populated via cooperative energy transfer from two adjacent sensitizers. The basic difference between ETU and CUC is that in CUC the activator does not have adequate long-lived intermediate energy levels compatible to that of the sensitizers. CUC occurs mainly in Yb^{3+}/RE^{3+} doped UC materials, where Yb^{3+} acts as cooperative sensitizer. The efficiency of CUC is lower than that of the ETU.

Based on energy transfer within $NaGdF_4$:Yb^{3+},Tm^{3+}@$NaGdF_4$:Ln^{3+} (Ln = Tb, Eu, Dy, and Sm) core-shell nanostructures, the EMU process (**Figure 2e**) was first proposed by Liu and cow-orkers [21] in 2011. The EMU process involves four types of luminescent centers, namely sensitizer, accumulator, migrators, and activator. The sensitizer/accumulator and the activator are confined in separate layers of the core-shell and connected by migrators [10]. The sensitizer first excited by ground state absorption and transfers its energy to an accumulator, promoting it to higher excited state. The accumulator should possess energy levels with longer lifetimes to accept the energy from the sensitizer. Then, energy migration takes place from higher excited state of accumulator to migrator, followed by migration of the excitation energy through the migrators via core-shell interface [10]. Finally, the migrated energy is trapped by an activator in the shell and emits UC luminescence.

4.2. Excited-state dynamics

The excited-state dynamics of RE ions involved in UC processes has been extensively investigated in several bulk materials and most of these are also applicable to their equivalent nanoscale systems. Quantitatively, the UC process can be described by a set of rate equations [4, 10] by taking into account all the population and depopulation pathways involved in the concerned system.

$$\frac{dN_i}{dt} = \sum population\,rate - \sum depopulation\,rate$$

As an example of establishing rate equations, the rate equations for UC process upon 980 nm light excitation in Er^{3+}-Yb^{3+} system are discussed below [22].

As the absorption cross-section of Yb^{3+} is much larger than that of Er^{3+} at 980 nm excitation wavelength, it is reasonable to consider the energy transfer from Yb^{3+} to Er^{3+} [9]. The three possible energy ETU processes from Yb^{3+} to Er^{3+} are the following (refer to **Figure 3**):

(a) ETU-1: $^2F_{5/2}$ (Yb^{3+}) + $^4I_{15/2}$ (Er^{3+}) $\rightarrow$ $^2F_{7/2}$ (Yb^{3+}) + $^4I_{11/2}$ (Er^{3+})

(b) ETU-2: $^2F_{5/2}$ (Yb^{3+}) + $^4I_{11/2}$ (Er^{3+}) $\rightarrow$ $^2F_{7/2}$ (Yb^{3+}) + $^4F_{7/2}$ (Er^{3+})

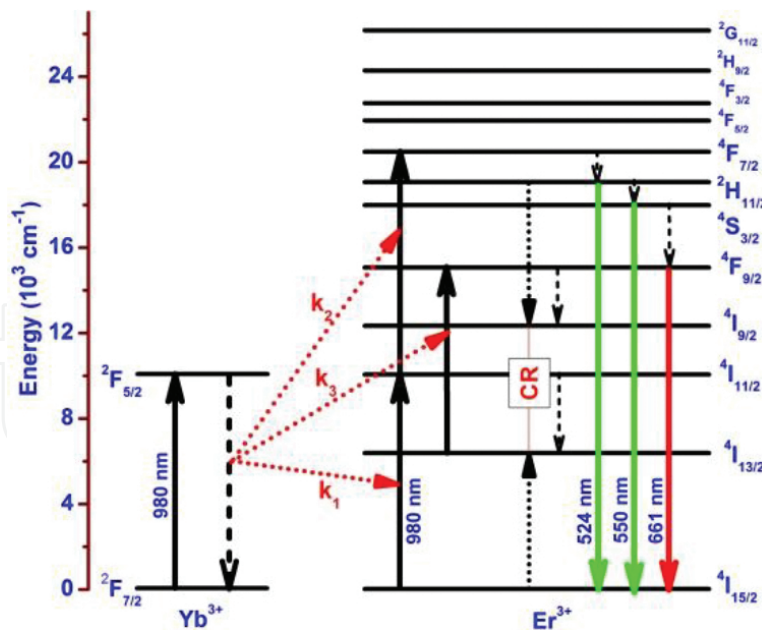(c) ETU-3: $^2F_{5/2}$ (Yb^{3+}) + $^4I_{13/2}$ (Er^{3+}) $\rightarrow$ $^2F_{7/2}$ (Yb^{3+}) + $^4F_{9/2}$ (Er^{3+})

Figure 3. Energy transfer processes relevant for upconversion in Er^{3+}-Yb^{3+} system [22].

The Er^{3+} ions raised to the $^4F_{7/2}$ level by ETU-2 relaxes nonradiatively to the $^2H_{11/2}$/$^4S_{3/2}$ levels and subsequently, radiative transition to the ground state ($^4I_{15/2}$) yields green UC emission bands. Possible mechanisms for population of the $^4I_{13/2}$ level of Er^{3+} are (i) energy back-transfer:

$^2H_{11/2}/^4S_{3/2}$ (Er^{3+}) + $^2F_{7/2}$ (Yb^{3+}) $\rightarrow$ $^4I_{13/2}$ (Er^{3+}) + $^2F_{5/2}$ (Yb^{3+}) and (ii) cross-relaxation process of Er^{3+} ions: $^2H_{11/2}/^4S_{3/2}$ + $^4I_{15/2}$ $\rightarrow$ $^4I_{9/2}$ + $^4I_{13/2}$.

The rate equations for Er^{3+}-Yb^{3+} codoped system are as follows:

$$\frac{dN_{Er,1}}{dt} = W_2 N_{Er,2} + C_{40} N_{Er,4} N_{Er,0} - k_3 N_{Er,1} N_{Yb,1} - W_1 N_{Er,1} - \rho_P \sigma_{13} N_{Er,1}$$

$$\frac{dN_{Er,2}}{dt} = k_1 N_{Er,0} N_{Yb,1} + \rho_P \sigma_{02} N_{Er,0} - k_2 N_{Er,2} N_{Yb,1} - W_2 N_{Er,2} - \rho_P \sigma_{24} N_{Er,2}$$

$$\frac{dN_{Er,3}}{dt} = k_3 N_{Er,1} N_{Yb,1} + \rho_P \sigma_{13} N_{Er,1} + W_4 N_{Er,4} - W'_3 N_{Er,3}$$

$$\frac{dN_{Er,4}}{dt} = k_2 N_{Er,2} N_{Yb,1} + \rho_P \sigma_{24} N_{Er,2} - W_4 N_{Er,4} - W'_4 N_{Er,4} - C_{40} N_{Er,4} N_{Er,0}$$

$$\frac{dN_{Yb,1}}{dt} = \rho_P \sigma_{Yb} N_{Yb,0} - \left(k_1 N_{Er,0} + k_2 N_{Er,2} + k_3 N_{Er,1} \right) N_{Yb,1} - W_{Yb} N_{Yb,1}$$

where $N_{Er,i}$ (i = 0, 1, 2, 3, 4) are the population densities of $^4I_{15/2}$, $^4I_{13/2}$, $^4I_{11/2}$, $^4F_{9/2}$ and $^2H_{11/2}/^4S_{3/2}$ levels of Er^{3+}. $N_{Yb,i}$ (i = 0, 1) are the population densities of the $^2F_{7/2}$ and $^2F_{5/2}$ levels of Yb^{3+}. W_1, W_2, and W_4 are the nonradiative decay rates of the $^4I_{13/2}$, $^4I_{11/2}$, and $^2H_{11/2}/^4S_{3/2}$ states, respectively; W'_3 and W'_4 are the radiative decay rates of the $^4F_{9/2}$ and $^2H_{11/2}/^4S_{3/2}$ states, respectively. The W_{Yb} is the radiative decay rate of the excited $^2F_{5/2}$ state of the Yb^{3+} ion. The k_1, k_2, and k_3 are the energy transfer rates of ETU-1, ETU-2, and ETU-3, respectively. The C_{40} is the cross-relaxation rate for $^2H_{11/2}/^4S_{3/2}$ + $^4I_{15/2}$ $\rightarrow$ $^4I_{9/2}$ + $^4I_{13/2}$; σ_{ij} is the absorption cross-section between levels i and j of Er^{3+}; σ_{Yb} is the absorption cross-section between levels $^2F_{5/2}$ and $^2F_{7/2}$ of Yb^{3+} and ρ_P is the pump constant which is proportional to the incident pump power, I_P. If the absorption cross-section of Er^{3+} is low compared to that of Yb^{3+} at 980 nm, the contribution of ground state absorption and ESA processes of Er^{3+} states can be neglected in comparison to the ETU (by Yb^{3+}) and relevant terms can be excluded from the rate equations. The energy transfer rates can be calculated using Judd-Ofelt theory [23, 24]. The multiphonon nonradiative relaxation rates can be derived using the modified energy gap law [4]. Once the transition rates are known, the characteristics of UC, namely, luminescence lifetime, spectral ratios, and quantum yields can be determined by solving these rate equations.

The rate equation model for UC process is generally made for theoretical analysis, but only very few reports are available on the use of this approach in UC nanomaterials mainly due to the complex nature of the involved UC process at the nanoscale and most of the spectroscopic characteristics of UC nanoparticles are determined experimentally. The investigation into the

time-resolved photoluminescence behavior of UC emissions is often used to check the validity of the proposed model of UC processes, and the rate constants are extracted from the fittings [10]. The lifetime of the activator's excited state is shorter than those of the sensitizers. The ETU processes lengthen the lifetime of the activators due to energy transfer from the sensitizers. Thus, the apparent lifetime of the activators is dependent on the sensitizers. The measured lifetime in UC luminescence and downconversion luminescence (the excited states are directly excited) is different. However, in the nanomaterials several factors such as surface quenching effect, particle size, and surface structure affect the lifetime and deviate from the theoretical value. The UC process shows pump power-dependent UC luminescence due to its nonlinear character. The combination of pump power dependent of UC with the steady-state rate equations yields useful information on the UC kinetics. Theoretical models proposed by Pollnau et al. and Suyver et al. [25, 26] are used vastly to know the nature of UC, i.e., the number of photons absorbed in the UC processes. The UC emission intensity (I) is proportional to nth orders of the pump power density (P): $I \propto P^n$, where 'n' is the number of photons absorbed in the particular UC process. Thus, the slope of the plot of $\ln[I]$ vs. $\ln[P]$ reveals the nature of the UC process. The pump power dependence of the UC emission is valid in low power density and becomes complicated at high pump power due to the competition between linear decays and UC processes. In most of the cases, the slope value decreases with increasing excitation power and at very high pump power, the UC processes sometimes become pump independent due to saturation of some intermediate levels.

4.3. Photophysical processes

Basic understanding of the main photophysical processes of UC emission is necessary not only for design and optimization of performance of UC materials but also the proper interpretation of experimental results. Although the three major steps photon absorption, subsequent energy transfer, and emission of UC are key processes, various nonradiative processes that compete with the radiative processes play vital roles in determining UC efficiency. Luminescence intensities are connected to the quantum-mechanical transition rates that depend on the details of the energy states that take part for the particular UC emission. The details of the initial and final states involved in the UC emission can be determined by Judd-Ofelt theory [23, 24]. This theory is based on the approximation that all the Stark manifolds have equal population and the host matrix element is isotropic. This approach facilitates to estimate the radiative rates for RE^{3+} ions theoretically by using the experimental parameters of optical absorption or emission spectra. The radiative decay rate, W_{rad} (photons/s) for an electric dipole allowed transition between two manifolds of RE^{3+} ion can be described as [10]:

$$W_{rad} = \frac{4e^2\omega^3}{3\hbar c^3} \frac{1}{2J+1} n \left(\frac{n^2+2}{3}\right)^2 \sum_{\lambda=2,4,6} \Omega_\lambda \left|\langle SLJ||U^{(\lambda)}||S'L'J'\rangle\right|^2$$

where $|SLJ\rangle$ and $|S'L'J'\rangle$ are the initial and final states of the transition, respectively. e, ω, $\hbar$, c, and n are the electronic charge, average angular frequency of the optical transition, reduced Planck constant, speed of light, and refractive index, respectively. $[(n^2+2)/3]^2$ is the Lorentz local field

correction factor, and $(2J + 1)$ is the degeneracy manifold of the initial state. $|\langle SLJ||U^{(\lambda)}||S'L'J'\rangle|^2$ are the squared matrix elements of the electric dipole operator between the initial and final manifolds. The Ω_λ (λ = 2, 4, 6) are Judd–Ofelt parameters that can be obtained from the optical absorption characterization of the material and give the influence of the host matrix on the electric dipole transition probabilities. In order to understand the UC mechanism involving 4f electrons more precisely, the magnetic dipole transitions which are weakly affected by the crystal field of the host should be combined to the Judd-Ofelt rates. With magnetic dipole transitions factored in, the Hamiltonian of a free ion (RE^{3+}) can be treated in quantifying the magnetic part of the UC emission in RE^{3+}.

Within a sensitizer-activator pair, the excitation energy of the sensitizer is transferred resonantly to adjacent activator. The resonant energy transfer process may be radiative or nonradiative. The nonradiative energy transfer takes place via long-range dipole-dipole interactions while the former one requires emission and reabsorption of a photon [10]. According to Dexter's theory [27], the resonant energy transfer probability W_{SA} between the sensitizer and activator ions can be expressed using the spectral overlap of the emission of sensitizer and absorption of activator. The energy transfer probability is given by [3]:

$$W_{SA} = \frac{3h^4c^4}{64\pi^5n^4\tau_S}\frac{Q_{abs}}{r_{SA}^6}\int\frac{f_{em}^S(E)f_{em}^A(E)}{E^4}dE$$

where h, c, n, r_{SA}, and τ_S are Planck's constant, the speed of light, the refractive index, the sensitizer-activator distance, and the intrinsic lifetime of the sensitizer, respectively; Q_{abs} is the integrated absorption cross-section of the activator ion, $f_{em}^A(E)$ and $f_{em}^S(E)$ are the normalized spectral functions of the absorption band of the activator at intermediate levels ($\int f_{em}^A(E)dE = 1$) and the emission band of the sensitizer at excited states ($\int f_{em}^S(E)dE = 1$), respectively [3, 10]. Therefore, the sensitizer-activator separation (r_{SA}) and the spectral overlap (the integration part) are the two key parameters governing the energy transfer. Another requirement to get efficient energy transfer is the high absorbance (Q_{abs}) of the activator ion at the emission wavelength of the sensitizer ion.

If there is an energy mismatch between the energy levels of the sensitizer and activator ions, the resonant energy transfer probability, W_{SA} decreases exponentially with the magnitude of the mismatch and the energy transfer will be no more resonant. Nevertheless, energy transfer in such case is compensated by the nonradiative, phonon-assisted processes, known as phonon-assisted energy transfer [3, 10].

5. Applications

UC materials have been extensively used in solid-state-lasers and waveguide amplifiers for a long time [3]. Applications in rewritable optical storage and nondestructive optical memory

devices are examples of some recent developments of exploiting UC materials in practical use [3]. Furthermore, the applications of these materials in biological field have been considered after the tremendous progress in preparation of UC nanomaterials with controllable particle size and shape. Recently, a diagnosis method for Ebola virus has been proposed by Tsang et al. using UC nanoparticles [28]. Therefore, advances of UC materials in newer applications will now be discussed in this section.

5.1. Lighting and displays

As a source of three primary colors—red, green and blue, UC emission offers many attractive features for display devices. An eminent advantage is the ability to operate displays with very high brightness and saturated colors without deterioration of the light emitting materials. Such displays are appropriate for high-brightness ambient lighting conditions.
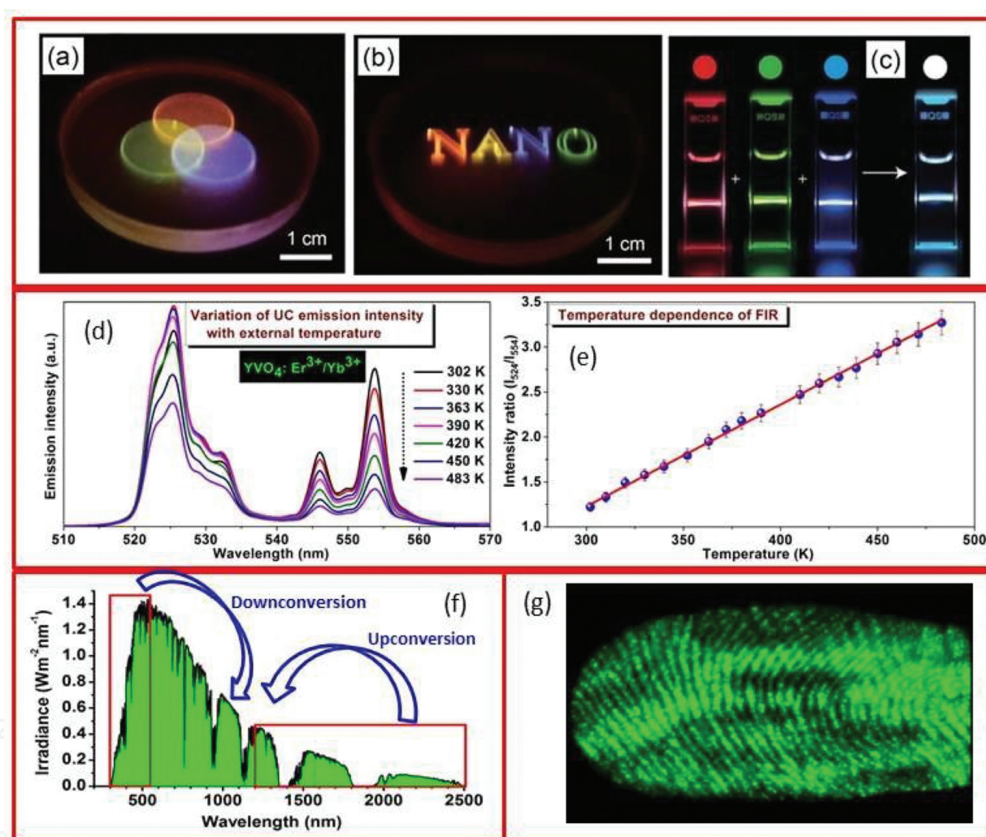

Figure 4. Luminescence color images generated in a RE-doped nanocrystal/polydimethylsiloxane composite monolith show the ability to display (a) additive colors [29], (b) three-dimensional objects [29], (c) volumetric three-dimensional display generated by combining three sets of conventional upconversion nanoparticles featuring monochromatic RGB emission (red, KMnF$_3$:Yb/Er; green, NaYF$_4$:Yb/Er; blue, NaYF$_4$:Yb/Tm) [29], (d) variation of UC emission intensity of green bands (524 nm and 554 nm) with external temperature of YVO$_4$:Er^{3+}/Yb^{3+} particles [36], (e) plot of fluorescence intensity ratio (FIR) as a function of external temperature [36], (f) AM1.5G solar irradiance spectrum (1000 W m^{-2}) and available for downconversion or downshifting (about 16% up to 500 nm) and upconversion (about 16% in the range of 1.2–2.5 μm), and (g) fresh fingerprint on glass by dry powdering with YVO$_4$:Er/Yb particles illuminated at 980 nm light [47]. Figures reproduced with permission from: (a–c) Ref. [29], Nature Publishing Group; (d and e) Ref. [36], Elsevier; and (g) Ref. [47], Optical Society of America.

The ability of dispersion of UC materials in polymers has further extended their applications in displays. For instance, $NaYF_4$:Er(Tm),Yb-PMMA nanocomposite producing white, blue, and green lights have been designed by Lin and his group [29] through *in situ* photopolymerization. Downing et al. [30] and Wang et al. [31] have shown that UC materials can be employed for three-dimensional displays. A very recent work by Deng et al. [32] shows the modulation of UC emission color of multilayer core-shell structure by controlling the pulse duration of the excitation laser. **Figure 4(a–c)** exhibits the volumetric three-dimensional display using pulse duration sensitive nanocrystals.

5.2. Temperature sensing

The luminescence from lanthanide-doped materials is an interesting solution to collect information about temperature in hazardous environment, microelectronic and photonic devices. Temperature sensing has been studied from the last decade using luminescent microcrystalline compounds at the tip of scanning thermal probe, at the tip of optical fiber or on the silica-on-silicon waveguides [33]. Although there were some drawbacks due to micron-sized particles; because the material may act as a thermal insulator and light scattering by rough surfaces of the bigger particles degrades the resolution of temperature sensing. The most important feature of UC nanoparticle-based thermometry is that these particles can be employed inside the cells. The temperature sensing of RE-doped UC materials is determined by two commonly used methods, i.e., decay time and fluorescence intensity ratio (FIR) methods. Besides these two major techniques, there are some other reports on temperature sensing based on temperature-dependent variation in emission bandwidth, variation of intensities of Stark sublevels, valley-to-peak intensity ratio, etc. [34, 35]. The most accepted method used for temperature sensing is based on the FIR technique which includes temperature-dependent variation of intensity ratio, emitted from two thermally coupled levels. The FIR method, in principle, uses low excitation power or short pulsed excitation in order to reduce the self-heating of the nanoparticles. The most studied RE element for temperature sensing application is Er^{3+}, which has well-known thermally coupled $^2H_{11/2}$ and $^4S_{3/2}$ levels. The sensor sensitivity is defined as the ratio in which the FIR changes with the temperature and is considered as the standard figure-of-merit. **Figure 4d** shows the upconversion spectra of an Er^{3+}, Yb^{3+} codoped YVO_4 powder recorded within 302–483 K [36]. The change in emission intensity from thermally coupled electronic multiplets is clearly observed. **Figure 4e** shows the plot of intensity ratio versus absolute temperature. As expected the system shows Boltzmann distribution of populations of the $^2H_{11/2}$ and $^4S_{3/2}$ levels. Among the luminescent thermometers proposed till now at submicron scale, only a few of them successfully illustrated the temperature sensing with a scanning microscope, e.g., thermal sensors using Er^{3+}/Yb^{3+} codoped fluoride glass [37] and $NaYF_4$:Er^{3+}/Yb^{3+} nanoparticles [38]. Temperature sensing performance up to 2000 K using metal-nanoparticle decorated, $(Gd,Yb,Er)_2O_3$ nanorods exploiting FIR technique and blackbody radiation has been reported recently by Carlos and his group [39].

5.3. Solar cell

Nonabundance of fossil fuel and public nonwillingness to accept nuclear power have encouraged researchers to search for alternative energy sources. Solar energy, a contemporary nonconventional source of energy is an obvious natural target due to its availability in large quantities. Crystalline silicon (c-Si) semiconductor was the key material for the earlier solar cells for converting solar energy into electricity. But the production of solar energy is still limited due to low efficiencies of power conversion. The multijunction semiconductor-based solar cells have maximum conversion efficiency 37.5% while the commercial silica-based solar cells have within 15–20% [40]. On the other hand, the dye-sensitized solar cells (DSSCs) yield conversion efficiencies below 12% [41]. The spectral mismatch between the incident photon energy of solar radiation and the band gap of c-Si semiconductor is one of the most important reasons for the low efficiency. Most of the solar energy is lost in several ways, including conversion to heat energy passing through the solar cell and thus it limits the efficiency [42, 43]. In order to enhance spectral response, wavelength converting layers are added to the solar cells. This layer is capable of absorbing the spectral range where photosensitive materials do not absorb well, although the addition of extra layers may modify the reflection, refraction and other optical responses in a negative or positive way. The photons of lower energy (UV/blue) can be converted into NIR through downconversion processes and NIR light can be upconverted by sequential absorption of two or more low-energy photons into visible or UV, which partially minimizes the optical mismatch in solar cells (**Figure 4f**). At the same time, the thermalization effect due to the carriers is greatly decreased and the conversion efficiency of the solar cell is enhanced. Nevertheless, examination of some available reports demonstrates that downshifting can add 1–2 absolute% to the conversion yield and upconversion 0.5–1% in silicon cells while in DSSC, the conversion yield is increased by 1–1.5% for downshifting and 0.2–0.5% for upconversion [44]. However, it is expected that these numbers will be increased in forthcoming years, especially if plasmonics are used to increase the UC efficiency.

5.4. Security

The unique properties of UC materials make them useful in security ink applications such as latent fingerprint and quick response code printing [45, 46]. Many UC particles are easily dispersible in well-known solvents, allowing printing or coating them onto various substrates. Moreover, multicolor emissions from UC layers upon IR excitation are useful for complex security patterns, giving another level of security or data protection. Earlier, we demonstrated the latent fingerprint detection (**Figure 4g**) using YVO_4:Er/Yb particles by a dry powdering method on a glass slide [47], which shows green fingerprint images upon 980 nm light illumination. The advantage of this technique is that it gives nearly no background and ridges can be detected clearly. The lifetimes of UC nanocrystals under a single-wavelength excitation vary from μs to ms and can be utilized for multiplexing in the time domain which is extendable to security and data storage technology including anticounterfeiting applications [48, 49].

5.5. Biomedical

With unique upconversion properties, UC nanoparticles yield high photostability, high sensitivity, and low optical background noise due to the absence of autofluorescence under NIR radiation which are suitable for bioimaging and biodetection [7, 28, 50, 51]. Moreover, NIR excitation enables deep penetration in tissue without damaging the biological specimens. Such properties of RE-doped UC nanomaterials are appropriate for a wide range of potential biological applications, including photodynamic therapy (PDT), drug delivery, biological imaging, and sensing. Most important point to be concerned for biomedical applications of UC nanomaterials is that the toxicity of the nanoparticles should be evaluated and must be nontoxic in nature for biological applications.

5.5.1. Biological imaging

The UC nanoparticle-based bioimaging has been widely used in cell, tissue, and small animal imaging due to their high contrast, absence of autofluorescence, and photostability against photobleaching and photoblinking [7, 50, 51]. The UC emissions are bright enough to be imaged at moderate excitation power of CW laser and can be used for single-molecule imaging. *In vitro* cellular imaging using RE-doped UC nanoparticles as targets has been demonstrated recently for colon cancer cells [52], ovarian cancer cells [53], HeLa cells [54], breast carcinoma cells [55], etc. In 2006, Lim and his coworkers [56] carried out pioneering work on live organism imaging on *Caenorhabditis elegans* worms using Y_2O_3:Er,Yb nanoparticles. The imaging of the digestive system of the worm under NIR excitation showed track of movement of the nano-particles in intestines. Besides organism imaging, *in vivo* imaging of small mammals has been studied using $NaYF_4$:Er,Yb nanoparticles by Chatterjee et al. [52] and demonstrated that the luminescence from the nanoparticles can be clearly observed upon NIR excitation even when the nanoparticles are placed ~10 mm beneath the skin of the animal and the study opens up a new perspective for bioimaging.

5.5.2. Biological sensing and detection

In biological sensing and detection [28, 57], UC luminescence is turned on or off by chromo-phoric complexes, decorated with the UC nanoparticles and the techniques are based on mainly two processes: fluorescence resonance energy transfer (FRET) and non-FRET [7]. The energy transfer in FRET takes place between donor and acceptor at a very short distance, typically shorter than 10 nm. Wang et al. [58] reported detection of avidin using human biotin-functionalized $NaYF_4$:Er/Yb and gold nanoparticles. Recently, Liu and his coworkers [59] proposed a highly sensitive biosensing platform based on UC nanoparticles and graphene as donor-acceptor system. On the other hand, in non-FRET based biological sensing, RE-doped UC nanoparticles are used as reporters and the luminescence from the nanoparticles is observed directly. Van de Rijke et al. [60] used Y_2O_2S:Er,Yb nanoparticles in the detection of nucleic acids and observed four-fold increase in the detection limit compared to conventional reporter.

5.5.3. Photodynamic therapy

The UC nanoparticles have recently been developed for application in cancer photodynamic therapy (PDT) [61–63]. For photodynamic therapy, three primary elements—excitation light, photosensitizer, and reactive oxygen species (ROS) are required. The photosensitizers are excited to the higher energy states under the irradiation of suitable NIR (**Figure 5**). The photosensitizer then returns to lower energy state producing energy which is transferred to the nearby oxygen and creates ROS that damages the cancer cells in the vicinity. Zhang et al. [64] first time designed the UC nanoparticles, coated with layer of mesoporous silica shell where the photosensitizers were doped for photodynamic therapy for the treatment of bladder cancer cells. Yan and his group [65] constructed $NaGdF_4$:Yb,Er@CaF_2 core/shell UC nanoparticles loaded with hematoporphyrin and silicon phthalocyanine dihydroxide molecules, and showed excellent PDT efficiency in HeLa cancer cells upon NIR irradiation.
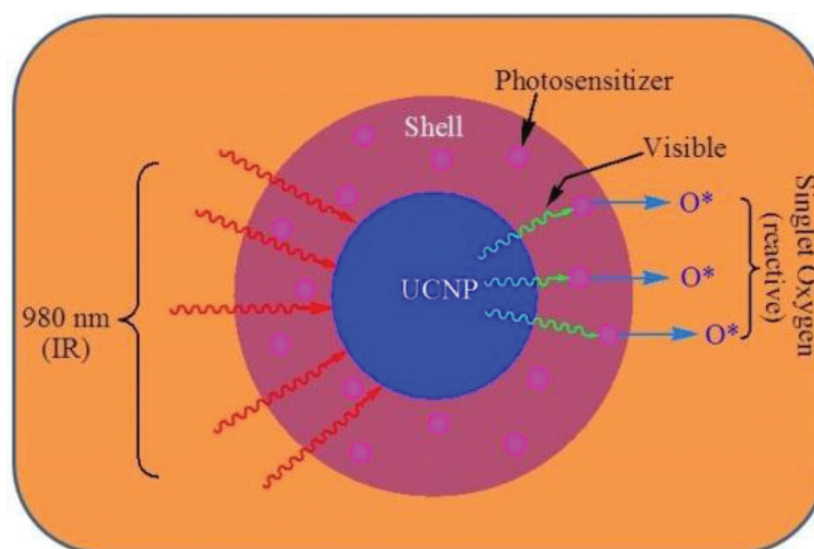

Figure 5. Schematic diagram of UC-based photodynamic therapy. The upconversion nanoparticles emit visible light which further excites the photosensitizers, resulting in the production of ROS and causes damage to the nearby cancer cells.

6. Summary and outlook

In summary, we presented an overview of the synthesis, properties, and recent development of RE-doped UC materials in various emerging applications. The UC materials show potential for a wide range of energy-related applications covering from lighting and display technologies to photovoltaic. At the same time, UC nanoparticles have proven to be effective in biological applications due to their unique optical and chemical properties such as absence of autofluorescence, low-toxicity, low photodamage to the biological cells, and high tissue-penetration depth of the excitation light. In spite of these benefits, there remain some limitations at the fundamental level associated with the practical use of UC materials. For example,

the efficiency of UC materials is restricted and to date, the maximum internal quantum yield has been obtained as 7.6% for $LiLuF_4$:Yb,Tm@$LiLuF_4$ [66] nanoparticles under NIR excitation. Another challenge for UC nanoparticles is surface engineering which is required for biomedical application and surface modification generally decreases the luminescence efficiency. Additionally, for biological applications, the UC nanoparticles should be the smallest (<10 nm) and the problem associated with smaller nanoparticles is that the upconversion efficiency decreases with decreasing particle size. However, manipulation of local environment around the RE ions in UC particles along with plasmons, quantum dots, dyes, or other dopants with a strong absorption might be effective ways to enhance the quantum yield. Therefore, more significant benefits of UC materials through constant and thriving research are yet to come in future for fundamental understanding as well as in emerging applications.

Acknowledgements

Author details

Manoj Kumar Mahata*, Hans Christian Hofsäss and Ulrich Vetter

*Address all correspondence to: mmahata@phys.uni-goettingen.de

Second Institute of Physics, University of Goettingen, Goettingen, Germany

References

[1] Bloembergen N. Solid state infrared quantum counters. Phys. Rev. Lett. 1959;2:84–85. DOI: 10.1103/PhysRevLett.2.84

[2] Auzel F. Upconversion and anti-Stokes processes with f and d ions in solids. Chem. Rev. 2004;104:139–173. DOI: 10.1021/cr020357g

[3] Zhou B., Shi B., Jin D., Liu X. Controlling upconversion nanocrystals for emerging applications. Nature Nanotech. 2015;10:924–936. DOI: 10.1038/NNANO.2015.251

[4] Zheng W., Huang P., Tu D., Ma E., Zhua H., Chen X. Lanthanide-doped upconversion nano-bioprobes: electronic structures, optical properties, and biodetection. Chem. Soc. Rev. 2015;44:1379–1415. DOI: 10.1039/c4cs00178h

[5] Walrand C. G., Binnemans K. Rationalization of crystal-field parametrization. In: Gscheidner Jr. K. A., Eyring L., editors. Handbook on the Physics and Chemistry of

Rare Earths. 23rd ed. Netherland: Elsevier Science B.V.; 1996. p. 121–283. DOI: 10.1016/S0168-1273(96)23006-5

[6]   Sun L. D., Dong H., Zhang P. Z., Yan C. H. Upconversion of Rare Earth Nanomaterials. Annu. Rev. Phys. Chem. 2015;66:619–642. DOI: 10.1146/annurev-physchem-040214-121344

[7]   Lin M., Zhao Y., Wang S. Q., Liu M., Duan Z. F., Chen Y. M. et al. Recent advances in synthesis and surface modification of lanthanide-doped upconversion nanoparticles for biomedical applications. Biotechnol. Adv. 2012;30(6):1551–1561. DOI: 10.1016/j.biotechadv.2012.04.009

[8]   Haase M., Schäfer H. Upconverting nanoparticles. Angew. Chem. Int. Ed. 2011;50:5808–5829. DOI: 10.1002/anie.201005159

[9]   Huang F., Liu X., Ma Y., Kang S., Hu L., Chen D. Origin of near to middle infrared luminescence and energy transfer process of Er^{3+}/Yb^{3+} co-doped fluorotellurite glasses under different excitations. Sci. Rep. 2015;5:8233(1–6). DOI: 10.1038/srep08233

[10] Nadort A., Zhao J., Goldys E. M. Lanthanide upconversion luminescence at the nanoscale: fundamentals and optical properties. Nanoscale. 2016;8:13099–13130. DOI: 10.1039/C5NR08477F

[11] Chang H., Xie J., Zhao B., Liu B., Xu S., Ren N. et al. Rare earth ion-doped upconversion nanocrystals: synthesis. Nanomaterials. 2015;5:1–25. DOI: 10.3390/nano5010001

[12] Mai H., Zhang, Y., Sun L., Yan C. Size- and phase-controlled synthesis of monodisperse $NaYF_4$:Yb,Er nanocrystals from a unique delayed nucleation pathway monitored with upconversion spectroscopy. J. Phys. Chem. C. 2007;111:13730–13739. DOI: 10.1021/jp073919e

[13] Yi G. S., Chow G. M. Colloidal LaF_3:Yb,Er, LaF_3:Yb,Ho and LaF_3:Yb,Tm nanocrystals with multicolor upconversion fluorescence. J. Mater. Chem. 2005;15:4460–4464. DOI: 10.1039/B508240D

[14] Mahata M. K., Kumar K., Rai V. K. Structural and optical properties of Er^{3+}/Yb^{3+} doped barium titanate phosphor prepared by co-precipitation method. Spectrochim. Acta A. 2014;124:285–291. DOI: 10.1016/j.saa.2014.01.014

[15] Mahata M. K., Koppe T., Hofsäss H., Kumar K., Vetter U. Host sensitized luminescence and time-resolved spectroscopy of YVO_4:Ho^{3+} nanocrystals. Phys. Procedia. 2015;76:125–131. DOI: 10.1016/j.phpro.2015.10.023

[16] Wu H., Xu H., Su Q., Chen T., Wu M. Size- and shape-tailored hydrothermal synthesis of YVO_4 crystals in ultra-wide pH range condition. J. Mater. Chem. 2011;13:1223–1228. DOI: 10.1039/B210713

[17] Zeng J. H., Su J., Li Z. H., Yan R. X., Li, Y. D. Synthesis and upconversion luminescence of hexagonal-phase NaYF$_4$:Yb^{3+},Er^{3+} phosphors of controlled size and morphology. Adv. Mater. 2005;17:2119–2123. DOI: 10.1002/adma.200402046

[18] Patra A., Friend C. S., Kapoor R., Prasad P. N. Fluorescence upconversion properties of Er^{3+}-doped TiO$_2$ and BaTiO$_3$ nanocrystallites. Chem. Mater. 2003;15:3650–3655. DOI: 10.1021/cm020897u

[19] Patra A., Friend C. S., Kapoor R., Prasad P. N. Upconversion in Er^{3+}:ZrO$_2$ nanocrystals. J. Phys. Chem. B. 2002;106:1909–1912. DOI: 10.1021/jp013576z

[20] Cheng Z. Y., Xing R. B., Hou Z. Y., Huang S. S., Lin J. Patterning of light-emitting YVO$_4$:Eu^{3+} thin films via inkjet printing. J. Phys. Chem. C. 2010;114:9883–9888. DOI: 10.1021/jp101941y

[21] Wang F., Deng R. R., Wang J., Wang Q. X., Han Y., Zhu H., et al. Tuning upconversion through energy migration in core-shell nanoparticles. Nat. Mater. 2011;10:968–973. DOI: 10.1038/nmat3149

[22] Mahata M. K., Koppe T., Mondal T., Bruesewitz C., Kumar K., Rai V. K., et al. Incorporation of Zn^{2+} ions into BaTiO$_3$:Er^{3+}/Yb^{3+} nanophosphor: an effective way to enhance upconversion, defect luminescence and temperature sensing. Phys. Chem. Chem. Phys. 2015;17:20741–20753. DOI: 10.1039/c5cp01874a

[23] Judd B. Optical absorption intensities of rare-earth ions. Phys. Rev. 1962;127(3):750–761. DOI: 10.1103/PhysRev.127.750

[24] Ofelt G. Intensities of crystal spectra of rare-earth ions. J. Chem. Phys. 1962;37 :511–520. DOI: 10.1063/1.1701366

[25] Pollnau M., Gamelin D., Lüthi S., Güdel H., Hehlen M. Power dependence of upconversion luminescence in lanthanide and transition-metal-ion systems. Phys. Rev. B: Condens. Matter. 2000;61:3337–3346. DOI: 10.1103/PhysRevB.61.3337

[26] Suyver J. F., Aebischer A., García-Revilla S., Gerner P., Güdel H. U. Anomalous power dependence of sensitized upconversion luminescence. Phys. Rev. B. 2005;71:125123. DOI: 10.1103/PhysRevB.71.125123

[27] Dexter D. L. A theory of sensitized luminescence in solids. J. Chem. Phys. 1953;21:836–850. DOI: 10.1063/1.1699044

[28] Tsang M. K., Ye W. W., Wang G., Li J., Yang M., Hao J. Ultrasensitive detection of Ebola virus oligonucleotide based on upconversion nanoprobe/nanoporous membrane system. ACS Nano. 2016;10(1):598–605. DOI: 10.1021/acsnano.5b05622

[29] Boyer J. C., Johnson N. J. J., van Veggel F. C. J. M. Upconverting lanthanide-doped NaYF4–PMMA polymer composites prepared by in situ polymerization. Chem. Mater. 2009;21(10):2010–2012. DOI: 10.1021/cm900756h

[30] Downing E., Hesselink L., Ralston J., Macfarlane R. A three-color, solid-state, three-dimensional display. Science. 1996;273(5279):1185–1189. DOI: 10.1126/science. 273.5279.1185

[31] Wang F., Han Y., Lim C. S., Lu Y. H., Wang J., Xu J., et al. Simultaneous phase and size control of upconversion nanocrystals through lanthanide doping. Nature. 2010;463:1061–1065. DOI: 10.1038/nature08777

[32] Deng R., Qin F., Chen F., Huang W., Hong M., Liu X. Temporal full-colour tuning through non-steady-state upconversion. Nat. Nanotechnol. 2015;10:237–242. DOI: 10.1038/nnano.2014.317

[33] Henry D. M., Herringer J. H., Djeu N. Response of 1.6 μm Er:$Y_3Al_5O_{12}$ fiber-optic temperature sensor up to 1520. Appl. Phys. Lett. 1999;74;3447. DOI: 10.1063/1.12412

[34] Soni A. K., Dey R., Rai V. K. Stark sublevels in Tm^{3+}–Yb^{3+} codoped Na2Y2B2O7 nano-phosphor for multifunctional application. RSC Adv. 2013;5:34999–35009. DOI: 10.1039/C4RA15891

[35] Li L., Xu W., Zheng L., Qin F., Zhou Y., Liang Z., et al. Valley-to-peak intensity ratio thermometry based on the red upconversion emission of Er^{3+}. Opt. Exp. 2016;24(12): 13244–13249. DOI: 10.1364/OE.24.013244

[36] Mahata M. K., Kumar K., Rai V. K. Er^{3+}–Yb^{3+} doped vanadate nanocrystals: a highly sensitive thermographic phosphor and its optical nanoheater behavior. Sensor Actuat. B-Chem. 2015;209:775–780. DOI: 10.1016/j.snb.2014.12.039

[37] Peng H. S., Stich M. I. J., Yu J. B., Sun L. N., Fischer L. H., Wolfbeis O. S. Luminescent europium(III) nanoparticles for sensing and imaging of temperature in the physiological range. Adv. Mater. 2010;22:716–719. DOI: 10.1002/adma.200901614

[38] Vetrone F., Naccache R., Zamarron A., Juarranz de la Fuente A., Sanz-Rodríguez F., Maestro L. M., et al. Temperature sensing using fluorescent nanothermometers. ACS Nano. 2010;4:3254–3258. DOI: 10.1021/nn100244a

[39] Debasu M. L., Ananias D., Pastoriza-Santos I., Liz-Marzan L. M., Rocha J., Carlos L. D. All-in-one optical heater-thermometer nanoplatform operative from 300 to 2000 K based on Er^{3+} emission and blackbody radiation. Adv. Mater. 2013;25:4868–4874. DOI: 10.1002/adma.201300892

[40] Green M. A., Emery K., Hishikawa Y., Warta W., Dunlop E. D. Progress in photovoltaics: research and applications. Photovoltaics. 2012;20:606–614. DOI: 10.1002/pip.2267

[41] Yella A., Lee H. W., Tsao H. N., Yi C. Y., Chandiran A. K., Nazeeruddin M. K., et al. Porphyrin-sensitized solar cells with cobalt (II/III)-based redox electrolyte exceed 12 percent efficiency. Science. 2011;334:629–634. DOI: 10.1126/science.1209688

[42] Hill S. P., Dilbeck T., Baduell E., Hanson K. Integrated photon upconversion solar cell via molecular self-assembled bilayers. ACS Energy Lett. 2016;1(1):3–8. DOI: 10.1021/acsenergylett.6b00001

[43] Rodríguez-Rodríguez H., Imanieh M. H., Lahoz F., Martín I. R. Analysis of the upconversion process in Tm3+ doped glasses for enhancement of the photocurrent in silicon solar cells. Sol. Energ. Mat. Sol. Cells. 2016;144:29–32. DOI: 10.1016/j.solmat.2015.08.017

[44] Bünzli J. C. G., Chauvin A. S. Lanthanides in Solar Energy Conversion. In: Bünzli J. C. G., Pecharsky V. K., editors. Handbook on the Physics and Chemistry of Rare Earths. 44th ed. Amsterdam: Elsevier Science, B.V.; 2014. p. 169–281. DOI: 10.1016/B978-0-444-62711-7.00261-9

[45] Wang J., Wei T., Li X., Zhang B., Wang J., Huang C., et al. Near-infrared-light-mediated imaging of latent fingerprints based on molecular recognition. Angew. Chem. Int. Ed. 2014;53:1616–1620. DOI: 10.1002/anie.201308843

[46] Meruga J. M., Baride A., Cross W., Kellar J. J., May P. S. Red-green-blue printing using luminescence-upconversion inks. J. Mater. Chem. C. 2014;2:2221–2227. DOI: 10.1039/C3TC32233E

[47] Mahata M. K., Tiwari S. P., Mukherjee S., Kumar K., Rai V. K. YVO$_4$:Er^{3+}/Yb^{3+} phosphor for multifunctional applications. J. Opt. Soc. Am. B. 2014;31(8):1814–1821. DOI: 10.1364/JOSAB.31.001814

[48] Gorris H. H., Wolfbeis O. S. Photon-upconverting nanoparticles for optical encoding and multiplexing of cells, biomolecules, and microspheres. Angew. Chem. Int. Ed. 2013;52:3584–3600. DOI: 10.1002/anie.201208196

[49] Kumar P., Singh S., Gupta B.K. . Future prospects of luminescent nanomaterial based security inks: from synthesis to anti-counterfeiting applications. Nanoscale. 2016;8:14297–14340. DOI: 10.1039/C5NR06965C

[50] Liu Y., Su Q., Zou X., Chen M., Feng W., Shi Y. et al. Near-infrared in vivo bioimaging using a molecular upconversion probe. Chem. Commun. 2016;52:7466–7469. DOI: 10.1039/C6CC03401B

[51] Tan G. R., Wang M., Hsu C.Y., Chen N., Zhang Y. Small upconverting fluorescent nanoparticles for biosensing and bioimaging. Adv. Opt. Mater. 2016;4(7):984–997. DOI: 10.1002/adom.201600141

[52] Chatterjee D. K., Rufaihah A. J., Zhang Y. Upconversion fluorescence imaging of cells and small animals using lanthanide doped nanocrystals. Biomaterials. 2008;29:937–943. DOI: 10.1016/j.biomaterials.2007.10.051

[53] Boyer J. C., Manseau M. P., Murray J. I., van Veggel F. C. J. M. Surface modification of upconverting NaYF4 nanoparticles doped with PEG-phosphate ligands for NIR (800 nm) biolabeling within the biological window. Langmuir. 2010;26:1157–1164. DOI: 10.1021/la902260j

[54] Cheng L., Yang K., Li Y. G., Chen J. H., Wang C. Y., Shao M. W., et al. Facile preparation of multifunctional upconversion nanoprobes for multimodal imaging and dual-targeted photothermal therapy. Angew. Chem. 2011;123:7523–7528. DOI: 10.1002/anie.201101447

[55] Yang Y. M., Shao Q., Deng R. R., Wang C., Teng X., Cheng K., et al. In vitro and in vivo uncaging and bioluminescence imaging by using photocaged upconversion nanoparticles. Angew. Chem. Int. Ed. 2012;51:3125–3129. DOI: 10.1002/anie.201107919

[56] Lim S. F., Riehn R., Ryu W. S., Khanarian N., Tung C. K., Tank D., et al. In vivo and scanning electron microscopy imaging of upconverting nanophosphors in *Caenorhabditis elegans*. Nano Lett. 2006;6:169–174. DOI: 10.1021/nl0519175

[57] Li H., Shi L., Sun D., Li P., Liu Z. Fluorescence resonance energy transfer biosensor between upconverting nanoparticles and palladium nanoparticles for ultrasensitive CEA detection. Biosens. Bioelectron. 2016;86:791–798. DOI: 10.1016/j.bios.2016.07.070

[58] Wang L. Y., Yan R. X., Huo Z. Y., Wang L., Zeng J. H., Bao J. et al. Fluorescence resonant energy transfer biosensor based on upconversion-luminescent nanoparticles. Angew. Chem. Int. Ed. 2005;44:6054–6057. DOI: 10.1002/anie.200501907

[59] Liu J., Liu Y., Liu Q., Li C., Sun L., Li F. Iridium(III) complex-coated nanosystem for ratiometric upconversion luminescence bioimaging of cyanide anions. J. Am. Chem. Soc. 2011;133:15276–15279. DOI: 10.1021/ja205907y

[60] van de Rijke F., Zijlmans H., Li S., Vail T., Raap A. K., Niedbala R. S. et al. Up-converting phosphor reporters for nucleic acid microarrays. Nature Biotechnol. 2001;19:273–276. DOI: doi: 10.1038/85734

[61] Dong H., Tang S., Hao Y., Yu H., Dai W., Zhao G. et al. Fluorescent MoS2 quantum dots: ultrasonic preparation, up-conversion and down-conversion bioimaging, and photodynamic therapy. ACS Appl. Mater. Interfaces. 2016;8(5):3107–3117. DOI: 10.1021/acsami.5b10459

[62] Lu F., Yang L., Ding Y., Zhu J. J. Highly emissive Nd^{3+}-sensitized multilayered upconversion nanoparticles for efficient 795 nm operated photodynamic therapy. Adv. Funct. Mater. 2016;26(26):4778–4785. DOI: 10.1002/adfm.201600464

[63] Chen J., Zhao J. X. Upconversion nanomaterials: synthesis, mechanism, and applications in sensing. Sensors. 2012;12:2414–2435. DOI: 10.3390/s120302414

[64] Zhang P., Rogelj S., Nguyen K., Wheeler D. Design of a highly sensitive and specific nucleotide sensor based on photon upconverting particles. J. Am. Chem. Soc. 2006;128:12410–12411. DOI: 10.1021/ja0644024

[65] Qiao X. F., Zhou J. C., Xiao J. W., Wang Y. F., Sun L. D., Yan C. H. Triple-functional core–shell structured upconversion luminescent nanoparticles covalently grafted with photosensitizer for luminescent, magnetic resonance imaging and photodynamic therapy in vitro. Nanoscale. 2012;4:4611–4623. DOI: 10.1039/C2NR30938F

[66] Huang P., Zheng W., Zhou, S., Tu D., Chen Z., Zhu H. et al. Lanthanide-doped LiLuF$_4$ upconversion nanoprobes for the detection of disease biomarkers. Angew. Chem. Int. Ed. 2015;53(5):1252–1257. DOI: 10.1002/anie.201309503